Vinnik, L., Kiselev, S., Weber, M., Oreshin, S., Makeyeva, L. (2012): Frozen and active seismic anisotropy beneath soutern Africa. - Geophysical Research Letters, 39, L08301

DOI: 10.1029/2012GL051326

Frozen and active seismic anisotropy beneath southern Africa

L. Vinnik,[1] S. Kiselev,[1] M. Weber,[2,3] S. Oreshin,[1] and L. Makeyeva[1]

Received 11 February 2012; accepted 16 February 2012; published 17 April 2012.

[1] P receiver functions from 23 stations of the SASE experiment in southern Africa are inverted simultaneously with SKS waveforms for azimuthal anisotropy in the upper mantle. Our analysis resolves the long-standing issue of depth dependence and origins of anisotropy beneath southern Africa. In the uppermost mantle we observe anisotropy with a nearly E-W fast direction, parallel to the trend of the Limpopo belt. This anisotropy may be frozen since the Archean. At a depth of 160 km the fast direction of anisotropy changes to 40° and becomes close to the recent plate motion direction. This transition is nearly coincident in depth with activation of dominant glide systems in olivine and with a pronounced change in other properties of the upper mantle. Another large change in the fast direction of anisotropy corresponds to the previously found low-S-velocity layer atop the 410-km discontinuity.
Citation: Vinnik, L., S. Kiselev, M. Weber, S. Oreshin, and L. Makeyeva (2012), Frozen and active seismic anisotropy beneath southern Africa, *Geophys. Res. Lett.*, *39*, L08301, doi:10.1029/2012GL051326.

1. Introduction

[2] Shear-wave splitting in the SKS seismic phase is of interest, because the related azimuthal anisotropy is caused by mantle flow [e.g., *Savage*, 1999; *Fouch and Rondenay*, 2006]. Anisotropy at different depths can be of different origins: frozen (in the mantle lithosphere) or induced by recent flow (in the sub-lithospheric zone). The SKS technique has poor depth resolution, and, as a rule, origins and depths of the observed splitting cannot be determined without additional data. In this paper we address the controversial issue of depth-localized shear-wave splitting beneath stable continental interiors by using seismic data from the SASE network in southern Africa (Figure 1). The lithosphere of southern Africa includes fragments of the oldest Earth's lithosphere: the Kaapvaal and Zimbabve cratons that are more than 2700 Myr old [*de Wit et al.*, 1992].

[3] The first measurements of shear-wave splitting in southern Africa [*Vinnik et al.*, 1995] revealed a nearly uniform fast direction of azimuthal anisotropy of 20°–40° clockwise from north, very similar to the absolute plate motion direction (APM) since the Jurassic in the hot-spot reference frame. This similarity suggested that the large-scale component of the observed anisotropy is in the sub-lithospheric depth range and related to the African plate motion.

[4] In 1997–1999 a bigger network of broad-band seismograph stations was installed in southern Africa (Figure 1). The data on shear-wave splitting derived from this network (Figure 1) show the same trend as reported previously, but with a larger variability. The fast direction of 65 ± 15° in the group of stations between 20°S and 25°S is close to the E-W trend of the Limpopo mobile belt within this region. A similarity between the fast direction of anisotropy and the tectonic trend was taken for evidence that anisotropy is in the 'geologic' layer (lithosphere), whereas the 'APM' layer (asthenosphere) is isotropic [*Silver et al.*, 2001]. In this study we address the same issue by using seismic indications of depth of anisotropy rather than tectonic arguments.

2. Method

[5] To evaluate azimuthal anisotropy as a function of depth, we invert jointly P receiver functions (PRFs) and SKS waveforms. Our treatment of the PRFs is based on harmonic decomposition of their transverse components in azimuth domain [*Kosarev et al.*, 1984]. The approach of *Kosarev et al.* [1984] was perfected by *Vinnik and Montagner* [1996], *Levin and Park* [1997], *Girardin and Farra* [1998], *Farra and Vinnik* [2000] and *Vinnik et al.* [2007]. The present work is based on the method of *Vinnik et al.* [2007], but we use a seismograph array instead of a single station. PRF is represented by projections on the axes P (or L), SV (or Q) and T [*Vinnik*, 1977]. Axis L is parallel to the principal P-wave particle motion direction in the wave propagation plane, Q is normal to L in the same plane, and T (transverse) is normal to both Q and L. In an isotropic laterally homogeneous Earth the L component is coupled only with Q and there is no signal in the T component. In the presence of azimuthal anisotropy or/and lateral heterogeneity, the converted and reflected phases are recorded in all three components.

[6] We assume that the anisotropy is hexagonal with a horizontal or tilted symmetry axis. Other symmetries can be present in the Earth, but hexagonal symmetry is the simplest and able to capture the main observable effects in the real Earth [*Becker et al.*, 2006]. The isotropic component of the model is described by velocities Vp, Vs and density ρ. For the model with a horizontal symmetry axis, the anisotropic component is defined by the values of dVp/Vp, dVs/Vs, η and azimuth of the fast direction. Here dVp is the difference between the fast and slow P velocities, dVs is the same but for the S velocities, and η controls velocities for the directions intermediate between the fast and slow. Anisotropic components of SV and T vary in the azimuth domain with a dominant period of 180°. Then evaluation of the second azimuthal harmonics of the T and Q components of PRFs may isolate the effect of anisotropy.

[1]Institute of Physics of the Earth, Moscow, Russia.
[2]Deutsches GeoForschungsZentrum, Potsdam, Germany.
[3]Institut für Erd- und Umweltwissenschaften, Universität Potsdam, Potsdam, Germany.

0094-8276/12/2012GL051326

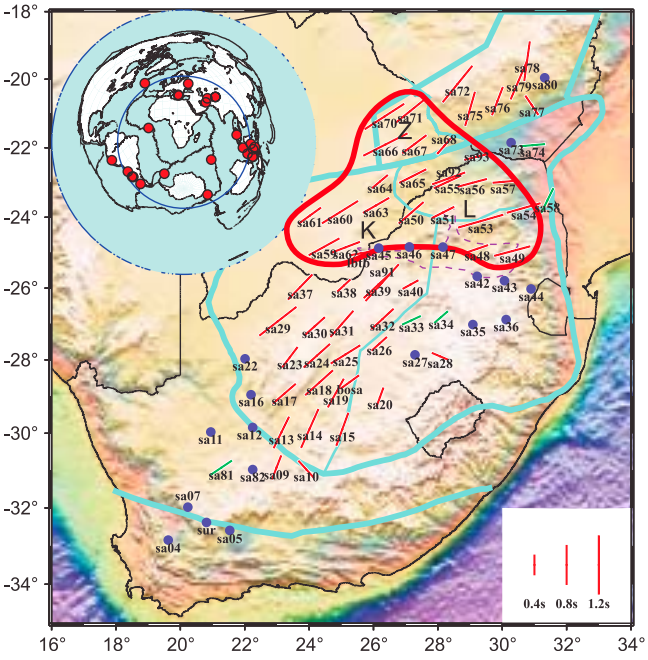

Figure 1. Shear-wave splitting data from SASE (adopted from *Silver et al.* [2001]). Orientation and length of bars give fast direction of anisotropy and splitting delay time. The stations without detectable splitting are shown by purple dots. Our study region is outlined in red. L, Z and K are for the Limpopo belt, Zimbabve craton and Kaapvaal craton. Inset: epicenters of earthquakes for PRFs.

[7] If the PRFs are obtained for discrete values of the back azimuth φ_i the second azimuthal harmonic can be evaluated by summation of the components of individual PRFs with weights depending on the azimuth. For the $T_i(t)$ and $Q_i(t)$ components, where t is time, we define weighting coefficients $W_T(i, \psi)$ and $W_Q(i, \psi)$:

$$W_T(i,\psi) = -\cos 2(\psi - \varphi_i)/\sum \cos^2 2(\psi - \varphi_i)$$
$$W_Q(i,\psi) = \sin 2(\psi - \varphi_i)/\sum \sin^2 2(\psi - \varphi_i)$$

The sums of $T_i(t)$ and $Q_i(t)$ are obtained as

$$F_T(t,\psi) = \sum W_T(i,\psi) T_i(t)$$
$$F_Q(t,\psi) = \sum W_Q(i,\psi) Q_i(t)$$

If the seismic events differ in the epicentral distance, the summation procedure may require move-out corrections on the order of 1 s for the individual PRFs, but in the depth range of our analysis (0–400 km) and at periods around 10 s the effect of the corrections is small enough to be neglected.

[8] Under the assumption of perfect separation of the second and the other azimuthal harmonics by the summation procedure the values of $F_T(t, \psi)$ and $F_Q(t, \psi)$ are similar [*Girardin and Farra*, 1998], and this similarity can be used as a criterion for azimuthal anisotropy. Experiments with synthetic seismograms demonstrate that $F_T(t, \psi)$ and $F_Q(t, \psi)$ are insensitive to the dip of the symmetry axis [*Girardin and Farra*, 1998; *Vinnik et al.*, 2007]. An efficient separation is important for $F_Q(t, \psi)$ because of a large amplitude of the 0-th (independent of the azimuth) harmonic, which is related to isotropic seismic boundaries in the crust and the upper mantle.

3. Data

[9] Correlation between $F_T(t, \psi)$ and $F_Q(t, \psi)$ is often found in seismic studies [e.g., *Girardin and Farra*, 1998; *Farra and Vinnik*, 2000; *Vinnik et al.*, 2007], but it is still unclear if this is sufficient for a robust discrimination between azimuthal anisotropy and lateral heterogeneity of isotropic medium. In the present study we reduce the effects of lateral heterogeneity by stacking recordings of 23 stations of the SASE network.

[10] The observations of splitting in SKS (Figure 1) reveal a few clusters of stations with relatively homogeneous fast directions within the cluster. At the southernmost group of stations (9, 13, 14, 15, 20) the azimuth of fast direction is 25 ± 5°. At a group of stations between 30°S and 25°S the fast direction is 45 ± 10°. At a group of stations between 25°S and 20°S the fast direction is between 50° and 80°, and at the northernmost stations the fast direction returns to the values at southern stations (~20°). The number of stations in the southernmost and northernmost groups is small, and the data are noisy. The second and third groups are larger, but a high signal/noise ratio (at least, 3) for $F_T(t, \psi)$ can be obtained only for the third group (outlined in red in Figure 1), and these data will be presented in detail.

[11] For every event and each motion component (Vert, W-E, S-N) all P-wave recordings were stacked with time shifts which removed differences in the arrival times, low-pass filtered with a corner period near 10 s, and the PRFs were calculated for the stacked motion components of each event. For some events the T component of the PRF thus obtained contained a small peak at 0 s time. This arrival is an effect of side refraction of the P wave or of errors in the horizontal-seismograph orientations, and it was eliminated by rotation of the horizontal axes to the appropriate back azimuth. The angle of rotation is, typically, ~3°. The rotation removes the peak at 0 s time, but practically does not affect other arrivals in the T component. The PRFs were calculated for 26 events (Figure S1 and Table S1 in the auxiliary material) for eleven back azimuths: 36°, 83°, 97°, 119°, 159°, 212°, 240°, 261°, 289.0°, 328° and 356°.[1] In the azimuthal sectors labeled 36°, 97°, 240° and 356° the resulting PRFs were obtained by stacking PRFs for several events, and the indicated azimuths are the average values. In each of the other azimuths there is only one well-recorded event. The PRFs were complemented by SKS recordings. The epicenters of events with a well recorded SKS phase form a few clusters. In our data set each cluster is represented by one event in the back azimuths of 99°, 269° and 328°. The R and T components of SKS were stacked within the sub-array, like the recordings of the P waves, but no receiver functions were computed for them.

[1]Auxiliary materials are available in the HTML. doi:10.1029/2012GL051326.

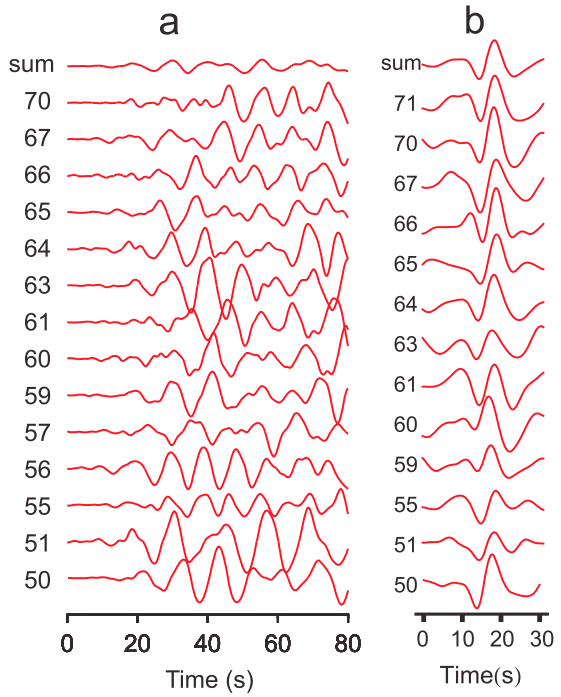

Figure 2. Examples of T-component recordings. (a) P-wave of earthquake of 25.03.1998; station numbers from Figure 1 are attached to the traces. (b) The same as in Figure 2a but for SKS phase of earthquake of 02.09.1997.

[12] A typical example of the T components of the P-wave (Figure 2a) shows that they have similar amplitudes (~0.08 or 8% of the P-wave amplitude), but are poorly correlated even at neighboring stations. As a result of the poor correlation, the amplitude of the average of all traces (trace 'sum') is around a quarter of those in the individual recordings. By comparison the T components of SKS (Figure 2b), which present a practically pure effect of anisotropy, are well correlated, and the trace 'sum' is comparable in amplitude with the other traces. This good correlation in addition to the data shown in Figure 1 testifies that the same anisotropy is common to all sites. Then a common anisotropic signal should be present in the shear phases which are generated by the P-wave in the upper mantle beneath the receivers. The wave-trains in individual recordings in Figure 2a are spatially incoherent and their amplitudes are too large to be anisotropy-related: their likely origin is related to small-scale heterogeneity in the vicinities of the seismograph stations. When these large and incoherent seismic phases are suppressed by stacking, the resulting signals (trace 'sum') can be easily reconciled with realistic anisotropy models.

[13] The T components of the PRFs for 11 azimuths (Figure S1 in the auxiliary material) consist of several interfering arrivals and, to be interpreted, require harmonic decomposition and inversion of $F_T(t, \psi)$ for the parameters of anisotropy. The obtained $F_T(t, \psi)$ (Figure 3a) contains a clear-cut wave-train with the maximum amplitude of less than 0.015 or 1.5% of the P wave amplitude. This amplitude is well above the noise arriving before or after the signal. Amplitudes of the first azimuthal harmonic (Figure 3b) are relatively small in the time interval from 5 s to 50s, corresponding to the upper-mantle depths, and the 'anisotropic' second harmonic in Figure 3a is clearly dominant. The first harmonic is dominant at small times corresponding to crustal depths.

[14] A similar analysis of the Q components reveals in several traces only marginal correlation between $F_T(t)$ and $F_Q(t)$. This is mainly the effect of a large, independent of the azimuth Q-component amplitude of the PRFs (~0.1 or 10% of the P-wave amplitude), insufficient suppression of the 0-th (independent of the azimuth) harmonic in $F_Q(t)$ and, most important, very small values of the second harmonic in our data. Strong suppression of the 0-th harmonic in $F_Q(t, \psi)$ requires a constant sampling rate of the P-wave recordings in back-azimuth domain, which is impossible with the available data. The actual suppression can be illustrated by the amplitude of $F_Q(t, \psi)$ for $Q_i(t)$ with similar waveforms and independent of the azimuth amplitudes of 0.1 (Figure 3c). The resulting amplitude of $F_Q(t, \psi)$ reaches 0.03 - about two times the maximum amplitude of $F_T(t, \psi)$ that can be used as a proxy for the second azimuthal harmonic, and this explains the large distortion of the second harmonic in $F_Q(t, \psi)$. However, in a window of ψ where $F_Q(t, \psi)$ in Figure 3c changes sign and approaches 0, there is a significant correlation between $F_T(t, \psi)$ and $F_Q(t, \psi)$ (Figure 3a), which may serve as a criterion of anisotropy.

[15] We invert $F_T(t, \psi)$ and SKS waveforms for azimuthal anisotropy by fitting the theoretical $F_T(t, \psi)$ and the T components of SKS to the observed functions with, practically, the same method as that of *Vinnik et al.* [2007]. For each trial model and each back azimuth we calculate synthetic $T_i(t)$ components of the PRFs by using the related L components as an input. The synthetic $T_i(t)$ are calculated with the Thomson-Haskell-Crampin algorithm [*Kosarev et al.*, 1979] and processed like the actual recordings. The theoretical T components of SKS are obtained with the same algorithm from the related radial components. We

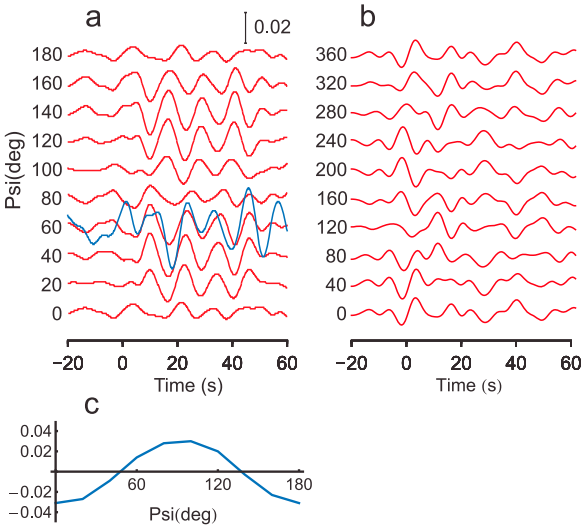

Figure 3. Results of harmonic decomposition: (a) $F_T(t, \psi)$ (red) and $F_Q(t, 60)$ (blue). Numbers on the left-hand side are values of ψ in degrees. The amplitude scale is relative to the P-wave amplitude. (b) The same as $F_T(t, \psi)$ in Figure 3a, but for the first azimuthal harmonic. (c) Amplitude of $F_Q(t, \psi)$ for the same back azimuths of earthquakes as in Figure S1 but for $Q_i(t)$ with the amplitude of 0.1 and a fixed waveform.

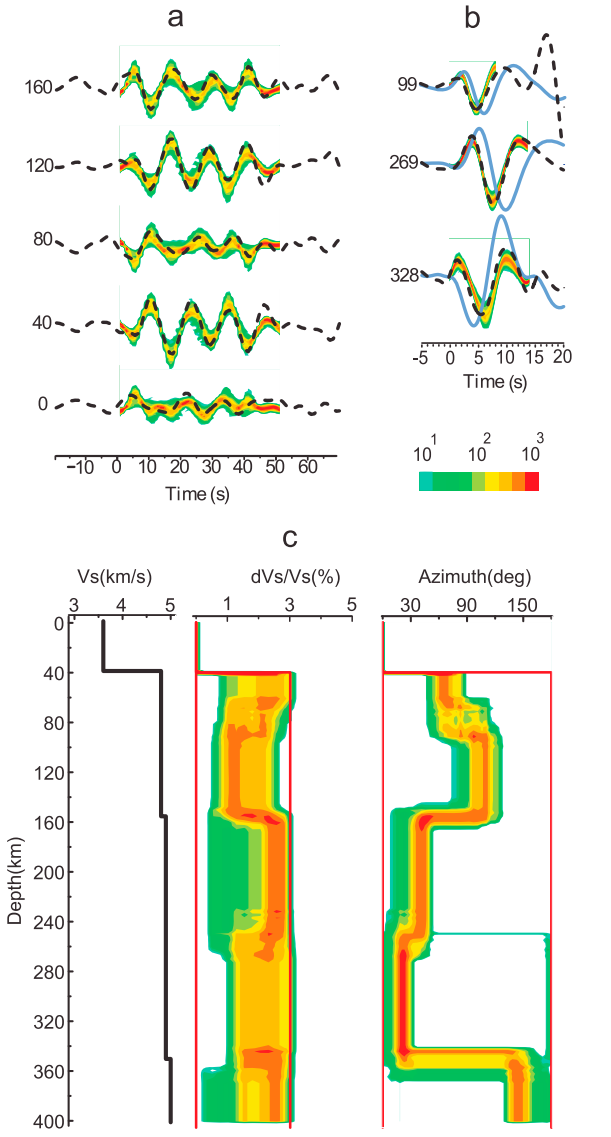

Figure 4. Inversion of $F_T(t, \psi)$ and SKS waveforms for azimuthal anisotropy. (a) $F_T(t, \psi)$ (dash lines) and histograms of synthetic $F_T(t, \psi)$ (color code) near the misfit minimum. Numbers on the left-hand side are values of ψ in degrees. (b) R (blue) and T (dash lines) components of SKS and histograms of synthetic T components (color code) near the misfit minimum; amplitudes of the R component are decremented 5 times. 99, 269 and 328 are back azimuths in degrees. (c) Isotropic S velocity model after Earth's flattening transformation (Vs), histograms of dVs/Vs and of fast direction (color code); red lines are limits of the search.

conduct a search for the optimum models by using an iterative algorithm, similar to simulated annealing [*Mosegaard and Vestergaard*, 1991], from 4 randomly selected starting points. The number of trial models for each starting point is 10^4. The last 2000 best-fitting models are used to evaluate a statistical distribution of the model parameters near the misfit minimum (Figure 4).

[16] The assumed isotropic velocities (Figure 4) correspond to shield models, smoothed and modified by the Earth's flattening transformation [*Biswas*, 1972]. Errors in the isotropic velocities lead to errors in the depth estimates for anisotropic models. Our tests suggest that these errors are less than 10 km. The crust is assumed to be isotropic with a thickness of 40 km. The unknowns in each mantle layer are dVs/Vs, the fast directions and the depths of the boundaries between the layers. The upper limit of dVs/Vs was set at 3%, in agreement with the estimates for kimberlite nodules from the Kaapvaal craton [*Ben-Ismail et al.*, 2001]. Following *Dziewonski and Anderson* [1981] we fixed η at 1.0 and verified that similar results can be obtained for $\eta = 0.95$. The effect of the ratio of (dVp/Vp)/(dVs/Vs) upon results of the inversion is negligible, and this ratio was fixed at 1.5. The search for the fast direction was in the range from 0 to 180°. The optimum model (Figure 4) includes 5 anisotropic layers. Between the Moho and a depth of 160 km the fast direction is from 70° to 105°. Between 160 km and 350 km, the fast direction is from 20° to 40°, and in a layer atop the 400-km discontinuity the direction is near 150° (or −30°). This model is insensitive to parametrization: the same main details are obtained for the stack of 12 anisotropic layers with a fixed thickness of 30 km (Figure S2 in the auxiliary material). Similar properties of the mantle are found in model with anisotropic crust (Figure S3). Our attempt to invert the first and second azimuthal harmonics (Figure 3) for anisotropy with dipping axes failed, and lateral heterogeneity presents the preferred explanation for the first harmonic.

4. Discussion and Conclusions

[17] The seismic data can be explained by a multi-layer mantle model (Figure 4) with the average mantle anisotropy around 2%, consistent with the properties of xenoliths [*Ben-Ismail et al.*, 2001]. In the uppermost 40 km of the mantle the fast direction is ~70°, close to the fast direction in SKS (Figure 1). This similarity is consistent with the modeling results which indicate that orientation of anisotropy in SKS tends to be weighted towards the orientations in the upper portions of the model [*Saltzer et al.*, 2000]. This fast direction is nearly parallel to the trend of the Limpopo belt which originated from the continental collision between the Kaapvaal and Zimbabve cratons at 2.7 Gyr [*de Wit et al.*, 1992]. A similar parallelism is often observed in the presently active collision zones like the Tien Shan, but at larger depths with higher temperatures [*Vinnik et al.*, 2007]. Then anisotropy at shallow depths beneath the Limpopo belt may imply a higher by ~400°C uppermost-mantle temperature in Archean relative to the present ~500°C [*Jones*, 1988]. At a depth of 80 km the fast direction changes to ~105°, but anisotropy becomes twice weaker.

[18] A major transition occurs at a depth of 160 km, where the fast direction changes to ~40° and anisotropy becomes at least twice as large. The temperature of ~900°C which activates dominant glide systems in olivine [*Estey and Douglas*, 1986] is reached at a depth of 130–150 km [*Jones*, 1988], close to 160 km. The change of the anisotropy at this depth is very likely caused by the transition from fossil anisotropy to the effect of the present-day flow. The "seismic" lithosphere/asthenosphere boundary, representing a transition from high (~4.7 km/s) to relatively low (4.5 km/s) S-wave velocities is found in about the same depth range [*Li and Burke*, 2006; *Priestley et al.*, 2006;

Wang et al., 2008; *Hansen et al.*, 2009; *Vinnik et al.*, 2009]. High-temperature (sheared) lherzolites in mantle xenoliths from the Kaapvaal craton originate at depths of 180–200 km [*James et al.*, 2004], within the layer of active anisotropy. Note that the mantle root of the craton may extend to a depth of 275 km [*Kuskov and Kronrod*, 2007]. Anisotropy similar to that found below 160 km, is predicted by *Forte et al.* [2010] from geodynamic modeling; the rate of the related flow is much greater than of overlying African plate motion. Anisotropy with the fast axis parallel to plate motion direction has been found in this depth range beneath the North-American craton [*Vinnik et al.*, 1992; *Marone and Romanowicz*, 2007] and the Siberian craton [*Oreshin et al.*, 2002].

[19] A change of the fast direction from 20° to −30° occurs at a depth of 350 km which corresponds to the upper boundary of the low-S-velocity layer atop the 410-km discontinuity beneath southern Africa [*Vinnik and Farra*, 2002]. This layer was detected by P and S receiver functions for seismic events from NE with the conclusion that the observed azimuthal dependence is an effect of anisotropy [*Vinnik et al.*, 2009]. The lowest velocity in our model is in the azimuth of 60°, consistent with the observations of *Vinnik et al.* [2009]. The low velocity and the change of the fast direction can both be effects of melting [*Hier-Majumder and Courtier*, 2011; *Holtzman et al.*, 2003].

[20] Estimates of the amplitude of $F_T(t, \psi)$ and of the related anisotropy for isolated stations in other regions are usually large relative to those in our study. For example, the amplitude of $F_T(t, \psi)$ at a station in Australia is 7.5% of the P-wave amplitude [*Girardin and Farra*, 1998] or 5 times the estimate for southern Africa. This difference implies either large lateral variations of anisotropy or contamination of $F_T(t, \psi)$ at isolated stations by effects of lateral heterogeneity. This issue can be resolved by applying our techniques in other regions.

[21] **Acknowledgments.** The Russian participants were partly supported by the RFBR grant 10-05-00879. The recordings of SASE were obtained from IRIS DMC. The authors thank Martha Savage and an anonymous reviewer for helpful comments.

References

Becker, T. W., S. Chevrot, V. Schulte-Pelkum, and D. K. Blackmann (2006), Statistical properties of seismic anisotropy predicted by upper mantle geodynamic models, *J. Geophys. Res.*, *111*, B08309, doi:10.1029/2005JB004095.

Ben-Ismail, W., G. Barruol, and D. Mainprice (2001), The Kaapvval craton seismic anisotropy: Petrophysical analyses of upper mantle kimberlite nodules, *Geophys. Res. Lett.*, *28*(13), 2497–2500, doi:10.1029/2000GL012419.

Biswas, N. N. (1972), Earth-flattening procedure for the propagation of Rayleigh wave, *Pure Appl. Geophys.*, *96*, 61–74, doi:10.1007/BF00875629.

de Wit, M. J., et al. (1992), Formation of an Archean continent, *Nature*, *357*(6379), 553–562, doi:10.1038/357553a0.

Dziewonski, A., and D. Anderson (1981), Preliminary reference Earth model, *Phys. Earth Planet. Inter.*, *25*(4), 297–356, doi:10.1016/0031-9201(81)90046-7.

Estey, L. H., and B. J. Douglas (1986), Upper-mantle anisotropy: A preliminary model, *J. Geophys. Res.*, *91*, 11,393–11,406, doi:10.1029/JB091iB11p11393.

Farra, V., and L. Vinnik (2000), Upper mantle stratification by P and S receiver functions, *Geophys. J. Int.*, *141*, 699–712, doi:10.1046/j.1365-246x.2000.00118.x.

Forte, A. M., S. Quere, R. Moucha, N. A. Simmons, S. P. Grand, J. X. Mitrovica, and D. B. Rowly (2010), Joint seismic-geodynamic-mineral physical modeling of African geodynamics: A reconciliation of deep-mantle convection with surface geophysical constraints, *Earth Planet. Sci. Lett.*, *295*(3–4), 329–341, doi:10.1016/j.epsl.2010.03.017.

Fouch, M. J., and S. Rondenay (2006), Seismic anisotropy beneath stable continental interiors, *Phys. Earth Planet. Inter.*, *158*(2–4), 292–320, doi:10.1016/j.pepi.2006.03.024.

Girardin, N., and V. Farra (1998), Azimuthal anisotropy in the upper mantle from observations of P-to-S converted phases: Application to southern Australia, *Geophys. J. Int.*, *133*(3), 615–629, doi:10.1046/j.1365-246X.1998.00525.x.

Hansen, S. E., A. A. Nyblade, J. Julia, P. H. G. M. Dirks, and R. J. Durrheim (2009), Upper-mantle low-velocity zone structure beneath the Kaapvaal craton from S-wave receiver functions, *Geophys. J. Int.*, *178*(2), 1021–1027, doi:10.1111/j.1365-246X.2009.04178.x.

Hier-Majumder, S., and A. Courtier (2011), Seismic signature of small melt fraction atop the transition zone, *Earth Planet. Sci. Lett.*, *308*(3–4), 334–342, doi:10.1016/j.epsl.2011.05.055.

Holtzman, B. K., D. L. Kohlstedt, M. E. Zimmerman, F. Heidelbach, T. Hiraga, and J. Hustoft (2003), Melt segregation and strain partitioning: Implications for seismic anisotropy and mantle flow, *Science*, *301*, 1227–1230, doi:10.1126/science.1087132.

James, D. E., F. R. Boyd, D. Schutt, D. R. Bell, and R. W. Carlson (2004), Xenolith constraints on seismic velocities in the upper mantle beneath southern Africa, *Geochem. Geophys. Geosyst.*, *5*, Q01002, doi:10.1029/2003GC000551.

Jones, M. Q. W. (1988), Heat flow in the Witwatersrand basins and environs and its significance for the South African shield geotherm and lithosphere thickness, *J. Geophys. Res.*, *93*(B4), 3243–3260, doi:10.1029/JB093iB04p03243.

Kosarev, G. L., L. I. Makeyeva, E. F. Savarensky, and E. M. Chesnokov (1979), Influence of anisotropy beneath seismograph station on body waves [in Russian], *Izv. Akad. Nauk Ser. Fiz. Zemli*, *2*, 26–37.

Kosarev, G. L., L. I. Makeyeva, and L. P. Vinnik (1984), Anisotropy of the mantle inferred from observations of P to SV converted waves, *Geophys. J. R. Astron. Soc.*, *76*, 209–220, doi:10.1111/j.1365-246X.1984.tb05037.x.

Kuskov, O. L., and V. A. Kronrod (2007), Composition, temperature, and thickness of the lithosphere of the Archean Kaapvaal craton, *Izv. Phys. Solid Earth*, *43*(1), 45–66.

Levin, V., and J. Park (1997), Crustal anisotropy in the Ural mountains foredeep from teleseismic receiver functions, *Geophys. Res. Lett.*, *24*, 1283–1286, doi:10.1029/97GL51321.

Li, A., and K. Burke (2006), Upper mantle structure of southern Africa from Rayleigh wave tomography, *J. Geophys. Res.*, *111*, B10303, doi:10.1029/2006JB004321.

Marone, F., and B. Romanowicz (2007), The depth distribution of azimuthal anisotropy in the continental upper mantle, *Nature*, *447*, 198–201, doi:10.1038/nature05742.

Mosegaard, K., and P. D. Vestergaard (1991), A simulated annealing approach to seismic model optimization with sparse prior information, *Geophys. Prospect.*, *39*, 599–611, doi:10.1111/j.1365-2478.1991.tb00331.x.

Oreshin, S., L. Vinnik, L. Makeyeva, G. Kosarev, R. Kind, and F. Wenzel (2002), Combined analysis of SKS splitting and regional traveltimes in Siberia, *Geophys. J. Int.*, *151*(2), 393–402, doi:10.1046/j.1365-246X.2002.01791.x.

Priestley, K., D. McKenzie, and E. Debayle (2006), The state of the upper mantle beneath southern Africa, *Tectonophysics*, *416*, 101–112, doi:10.1016/j.tecto.2005.11.024.

Saltzer, R. L., J. B. Gaherty, and T. S. Jordan (2000), How are vertical shear wave splitting measurements affected by variations in the orientation of azimuthal anisotropy with depth?, *Geophys. J. Int.*, *141*(2), 374–390, doi:10.1046/j.1365-246x.2000.00088.x.

Savage, M. K. (1999), Seismic anisotropy and mantle deformation: What have we learned from shear wave splitting?, *Rev. Geophys.*, *37*(1), 65–106, doi:10.1029/98RG02075.

Silver, P. G., S. S. Gao, and K. H. Liu, and the Kaapvaal Seismic Group (2001), Mantle deformation beneath southern Africa, *Geophys. Res. Lett.*, *28*(13), 2493–2496, doi:10.1029/2000GL012696.

Vinnik, L. (1977), Detection of waves converted from P to SV in the mantle. *Phys. Earth Planet. Inter.*, *15*, 39–45.

Vinnik, L., and V. Farra (2002), Subcratonic low-velocity layer and flood basalts, *Geophys. Res. Lett.*, *29*(4), 1049, doi:10.1029/2001GL014064.

Vinnik, L., and J.-P. Montagner (1996), Shear wave splitting in the mantle Ps phases, *Geophys. Res. Lett.*, *23*(18), 2449–2452, doi:10.1029/96GL02263.

Vinnik, L. P., L. I. Makeyeva, A. Milev, and A. Y. Usenko (1992), Global patterns of azimuthal anisotropy and deformations in the continental mantle, *Geophys. J. Int.*, *111*(3), 433–447, doi:10.1111/j.1365-246X.1992.tb02102.x.

Vinnik, L. P., R. W. E. Green, and O. Nicolaysen (1995), Recent deformation of the deep continental root beneath southern Africa, *Nature*, *375*, 50–52, doi:10.1038/375050a0.

Vinnik, L. P., I. M. Aleshin, S. G. Kiselev, G. L. Kosarev, and L. I. Makeyeva (2007), Depth localized azimuthal anisotropy from SKS and P receiver functions: The Tien Shan, *Geophys. J. Int.*, *169*(3), 1289–1299, doi:10.1111/j.1365-246X.2007.03394.x.

Vinnik, L., S. Oreshin, G. Kosarev, S. Kiselev, and L. Makeyeva (2009), Mantle anomalies beneath southern Africa: Evidence from seismic S and P receiver functions, *Geophys. J. Int.*, *179*(1), 279–298, doi:10.1111/j.1365-246X.2009.04261.x.

Wang, Y., L. Wen, and D. Weidner (2008), Upper mantle SH- and P-velocity structures and compositional models beneath southern Africa, *Earth Planet. Sci. Lett.*, *267*(3–4), 596–608, doi:10.1016/j.epsl.2007.12.010.

S. Kiselev, L. Makeyeva, S. Oreshin, and L. Vinnik, Institute of Physics of the Earth, B. Grouzinskaya 10, Moscow 123995, Russia. (vinnik@ifz.ru)

M. Weber, Deutsches GeoForschungsZentrum, Telegrafenberg, D-14473 Potsdam, Germany.